Effect of potassium and platinum contents on catalytic performance of Pt/Al2O3 monometallic catalysts for propane dehydrogenation

Alexandre van Assche, Catherine Especel, Anthony Le Valant, Florence Epron

Effect of potassium and platinum contents on catalytic performance of Pt/Al_2O_3 monometallic catalysts for propane dehydrogenation

*Alexandre Van Assche, Catherine Especel, Anthony Le Valant and Florence Epron**

Institut de Chimie des Milieux & Matériaux de Poitiers (IC2MP), Université de Poitiers, 4 rue Michel Brunet, TSA51106, 86073 Poitiers Cedex 9, France

Keywords: light alkane dehydrogenation, highly dispersed platinum, potassium, platinum catalyst, characterization of the acidity

Abstract (150words at max):

Low-loaded Pt-based catalysts supported on γ-Al_2O_3 (bare or modified by K) were studied for propane dehydrogenation. The alumina supported was modified by adding 0.5 and 4 wt.% of K using potassium acetate as precursor. 0.5 wt.% of K is sufficient for suppressing the acidity of the alumina. Ultradispersed Pt supported catalysts (0.1, 0.2 and 0.3 wt.%) were obtained by ion exchange on Al_2O_3 or Al_2O_3-0.5K. During propane dehydrogenation reaction, 0.3wt.%Pt/Al_2O_3 strongly deactivates, mainly due to coke deposition. For the same Pt loading, the presence of K strongly decreases this phenomenon without modifying the initial turnover frequencies (TOF). On the series supported on Al_2O_3-0.5K, there is no effect of the Pt content on the TOF values showing that whatever the sample, ultradispersed Pt entities present the same activity. Finally, the selectivity towards propene formation strongly depends on propane conversion and seems to be not affected by the change in K and Pt contents.

Highlights (max 85 characters including spaces)

- Low potassium loading is sufficient for suppressing alumina acidity.

- Catalysts with ultralow Pt contents lead to ultradispersed species.

- Ultradispersed Pt species are very active for propane dehydrogenation.

- The presence of potassium limits initial deactivation.

- Selectivity to propene depends on conversion with no effect of K and Pt contents.

Graphical abstract

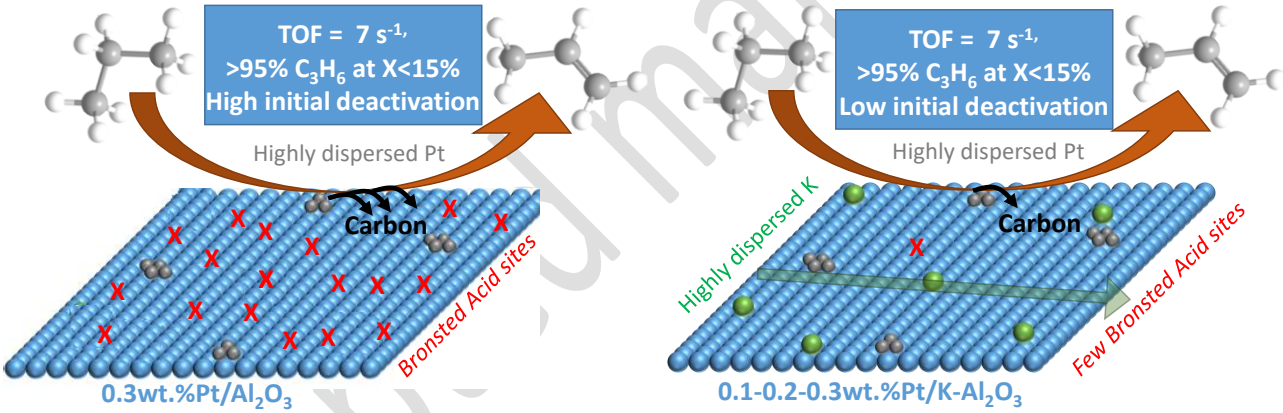

1. Introduction

Propylene is one of the most important building blocks for the production of a wide array of specialty chemicals such as polymers, resins, surfactants, dyes, and pharmaceuticals [1-8]. The supply of propylene has been reduced because of the recent shift in feedstock for steam crackers from naphtha to light alkanes, due to the scarceness of fossil fuels, the emergence of shale gas and the increasing availability of natural gas [1,9]. In this context, the direct propane dehydrogenation (PDH) is becoming a promising way to meet the increasing demand of propylene. The advantage of this process is the very high selectivity to propylene instead of a mixture of products compared to Fisher-Tropsch-to-olefins method for instance [6,10,11]. Nevertheless it is extremely energy intensive due to a high positive enthalpy of the reaction ($\Delta_r H^{\circ}_{298K}$°= 124 kJ mol^{-1}), necessitating high reaction temperatures (~ 550-700 °C) to achieve significant propane conversion. To date, two main technologies are used in industry *i.e.* Catofin® (Lummus, CrO_x-based catalysts) and Oleflex® (UOP, Pt-Sn bimetallic supported catalysts) [1]. Modified high surface area γ-Al_2O_3 is the classical support chosen for Pt-Sn dehydrogenation catalysts of the Oleflex® process, due to its high thermal stability, mechanical strength, low price, and ability of maintaining the Pt nanoparticles dispersion. Due to their high ability to activate paraffinic C-H bonds and their low activity to C-C cleavage avoiding side reactions, Pt-Sn on modified gamma alumina represents the most extensively studied system for non-oxidative dehydrogenation reaction [1,12,13]. On these catalysts, three types of side reactions can occur: (i) hydrogenolysis, catalysed by platinum sites leading to the formation of smaller alkanes; (ii) cracking resulting also in the cleavage of C-C bond but with no hydrogen required, involving generally Brønsted and Lewis acid sites of the alumina support; and (iii) isomerisation corresponding to a rearrangement of atoms and taking place mainly *via* a carbocation intermediate formed on a Brønsted acid sites [1]. High olefin yields can be obtained by carefully controlling the catalysts design and then the balance between dehydrogenation and side reactions, with the aim also of limiting the formation of coke

favoured under the high temperatures required in the process that leads to deactivation with time-on-stream.

In the literature, many efforts have been made to improve the activity and stability of Pt-Sn/γ-Al_2O_3 catalysts by loading them onto other porous supports, *i.e.* others types of Al_2O_3 (θ, mesoporous, 2D) [4,12,14,15], $MgAl_2O_4$ [16-18], SiO_2-SBA15 [12,19,20]. Various promoters such as B, Ga, Zn or Ce, for example, were also added to the alumina support in order to promote the catalytic activity and stability of supported Pt catalysts [1, 21, 22]. In order to decrease the acidity of the γ-Al_2O_3, which can lead to deep dehydrogenation, cracking and coke formation, an alkaline metal, such as Na or K, or alkaline-earth such as Mg, is often added to poison the acid sites [23,24]. In the literature, the effect of potassium content on the properties of Pt/Al_2O_3 catalysts has been only studied for oxidation reactions [25-29], and only one of them studied the modification of the acidity as a function of K content [29]. The acidity was determined from NH_3-TPD profiles, which do not allow to discriminate Brønsted from Lewis acid sites. It was demonstrated that K decreases the density of acidic sites, and that this decrease is more important for the largest amount of K [29]. However, to the best of our knowledge, the effect of these additives on the characteristics of alumina and on the catalytic properties for propane dehydrogenation remains few discussed in the literature where various additive loadings are found without real justification [30,31]. Furthermore, the catalytic performances (activity, selectivity, stability) of the Pt-Sn on modified γ-Al_2O_3 or other supports are explained in a general way on the basis of several properties linked to their preparation method, such as the metallic dispersion, the metal interaction, the presence of Pt-Sn alloys, tin reducibility and so on. In most cases, the platinum contents are mainly comprised between 0.5 [5,32,33] and 3 wt.% [7,34,35]. Surprisingly, due to their lower performances for propane dehydrogenation compared to Pt-Sn catalysts, the catalytic performances of monometallic Pt catalysts are the must often described for highlighting the better properties of the bimetallic systems [36,37]. Only few papers have been devoted to an in depth study of monometallic catalysts, and they were focused on the effect of Pt particle size on the catalytic performance. Even if

the dehydrogenation reaction of light alkanes is admitted to be insensitive to the structure of the Pt particles [1], so independent of the Pt particle size, it was reported that small particles deposited on Mg(Al)O hydrotalcite or SBA-15 are more active and less selective to propylene than the largest ones due to a higher activity to cracking products and coke formation leading to their deactivation [38,39]. More recently, an effect of particle size and metal loading was demonstrated on propane dehydrogenation reaction for Pt/Al_2O_3 catalysts, the lowest loading associated with the lowest Pt particle size leading to the most active catalysts, associated with a structure sensitivity [40]. All these studies were performed at platinum loadings of 1 wt.% or higher, and particle size ranges from 1 nm to more than 20 nm [38-40]. Nevertheless, the limited resource of Pt imposes to decrease as far as possible the metallic loading of the catalyst formulations, and Pt loadings of 0.3 wt.% or lower are used in the Oleflex® process. For these reasons, recent studies reported in the literature are increasingly focusing on low platinum contents [41-43].

In this context, the present paper is devoted to the study of Pt-based catalysts supported on γ-Al_2O_3 modified or not by addition of K (0.5 and 4 wt.%), containing a low metallic loading (from 0.3 to 0.1 wt.%), with the aim of understanding the effect of the K modifier and Pt content on their catalytic performances during propane dehydrogenation.

2. Experimental

2.1. Catalysts preparation

Supports

The support was a γ-alumina support (GOD200, Axens), with a surface area of 200 $m^2 g^{-1}$, crushed and sieved in order to obtain a granulometry between 250 and 100 μm. In order to modulate its acidity 5 g of support was impregnated using 20 mL of an aqueous solution of potassium precursor (CH_3COOK, Sigma-Aldrich) in order to obtain 0.5 and 4 wt.% of K at the alumina surface. After impregnation, excess of water was evaporated and the support was dried at 110 °C overnight. Thereafter, the alumina

support, alone (Al_2O_3) or modified by potassium (Al_2O_3-xK, where x is the nominal K content in wt.%), was calcined at 450 °C under air (60 mL min^{-1}) for 4 h (ramp of 10 °C min^{-1} for Al_2O_3 and 5 °C min^{-1} for Al_2O_3-K).

Catalysts

Pt/Al_2O_3 and Pt/Al_2O_3-K catalysts were prepared via the strong electrostatic adsorption (SEA) method [44].The support was put in contact with diammineplatinum (II) nitrite ($Pt(NH_3)_2(NO_2)_2$, 1.7 wt.% of Pt, Alfa Aesar) in 12 mL of aqueous solution at the initial pH of 11. The concentration of the platinum salt was adjusted in order to obtain catalysts with a nominal Pt content of 0.1, 0.2, and 0.3 wt.%. In the following, catalysts will be named yPt/Al_2O_3(-xK) where y is the nominal Pt content in wt.%. The slurry was shaken for one night and the sample was then filtrated, washed 3 times with 12 mL of aqueous solution at pH of 11. After drying at 100 °C for 1 night, the catalyst was calcined in air (60 mL min^{-1}) for 3 h at 450 °C, and reduced under hydrogen (60 mL min^{-1}) at 650 °C during 1 h. This reduction temperature was chosen to be slightly higher than the catalytic test temperature. Thus, the characteristics of the activated catalysts are representative of those of the catalysts at the beginning of the catalytic test. The final powder was sieved between 250 and 100 μm.

2.2. Characterization

BET surface area

The BET surface area was determined by N_2 adsorption using a Micromeritics Tristar II PLUS. Nitrogen adsorption experiments were performed at -196 °C. The specific surface area of the various catalysts was determined from the Brunauer-Emmet-Teller (BET) equation.

X-Ray diffraction

Powder X-Ray diffraction (XRD) patterns were recorded on a PANalytical EMPYREAN apparatus with a Cu Kα radiation (λ_1=1.5406 Å) and an X'Celerator detector. Data were collected over a range

of 15°-110° with 0.1° steps and a dwell time of 900 s. Crystalline phases present in the samples were identified by comparison with standards of the JCPDS database.

Determination of the metal content

Inductively coupled plasma optical emission spectroscopy (ICP-OES) was used for the determination of metal content of each sample. The measurements were performed with a Perkin Elmer Optima 2000DV spectrometer. The samples were previously digested in an acidic mixture of HNO_3 and HCl under microwave heating.

Transmission electron microscopy

Transmission electron microscopy (TEM) was performed with a JEOL 2100 UHR microscope equipped with an energy dispersive X-ray (EDX). The reduced catalysts were ultrasonically dispersed in ethanol and the suspension was brought onto a copper grid with carbon film. The metal particles were counted for each catalyst using the free software ImageJ®.

Determination of the carbon content by elemental analysis

The amount of carbon deposited, after the catalytic test, was determined by elemental analysis (Flash EA 1112, Thermoelectron).

Thermogravimetric analysis

Thermogravimetric (TG) and derivative thermogravimetric (DTG) analyses were used to characterize the bare alumina support as well as catalysts after catalytic test, using a Q600TA Instrument apparatus, under dry air, with a heating rate of 5 °C min^{-1} from room temperature to 900 °C.

Characterization of the acid sites

The Lewis acidity was evaluated using pyridine adsorption and desorption at 150, 250 and 350 °C followed by infrared spectrometry in a Thermo Nicolet Nexus equipment. The sample was pressed in

order to obtain a self-supported wafer of 20-25 mg with a diameter of 16 mm. The sample was then introduced in an *in situ* cell and pretreated at 500 °C in vacuum (10^{-6} bar) one night. Then the temperature was decreased at 150 °C and the reference spectrum was measured. This reference spectrum was analysed in the OH region. Then, the pyridine was introduced in the cell for 5 min. Then, the cell was evacuated to 10^{-6} bar. After 1 h in vacuum, the spectrum was recorded at 150 °C to determine the total number of acid sites. Then, the temperature was increased and spectra were recorded at 250 and 350 °C after evacuation for 1 h at each temperature. All the spectra were compared at a normalized sample weight of 20 mg. The amount of Lewis acid sites was determined from the integrated area using the value of the molar extinction coefficient (1.28 cm μmol^{-1}) of the band at 1455 cm^{-1} determined by Guisnet *et al.* [45], in the same conditions. The spectrum obtained at 150 °C was used to calculate the total amount of Lewis acid sites (LAS). The distribution of weak acid sites was calculated by difference between the surface area at 150 and 250 °C, the medium acid sites between 250 and 350 °C, while the amount of strong acid sites was directly determined from the spectrum at 350 °C.

The model reaction of 3,3-dimethylbut-1-ene (33DMB1) isomerization was used to characterize the weak Brønsted acid sites since the Lewis centres of alumina are not involved in this reaction [46,47]. Catalyst samples (0.1 g) were treated in flowing air (60 mL min^{-1}) at 450 °C, then in flowing hydrogen (60 mL min^{-1}) at 650 °C during 1 h and then purged under nitrogen. These reaction conditions were chosen in order to be similar to the ones used for the catalyst pretreatment before propane dehydrogenation test. The 33DMB1 isomerization reaction was carried out at 275 °C under a constant flow of 30 mL min^{-1} of N_2 saturated with 33DMB1. Isomerization products, 2,3-dimethyl-2-butene and 2,3-dimethyl-1-butene, as well as 33DMB1, were analysed by on-line gas chromatography. As this reaction was used to qualitatively evaluate the modifications induced by the deposition of potassium, ammonia and platinum on the Brønsted acidity of alumina, the catalysts and supports were compared in terms of relative activity as the following:

$$a_{rel.isom}(\%) = \frac{a_{isom}\,(x)}{a_{isom}\,(Al_2O_3)} \times 100 \qquad \text{(Eq. 1)}$$

where $a_{rel.isom}(\%)$ is the relative activity in % of sample x, $a_{isom}\,(x)$ and $a_{isom}\,(Al_2O_3)$ are the initial activity of x and Al_2O_3 samples (in mmol h^{-1} g^{-1}), respectively.

Catalytic test

Propane dehydrogenation reaction was carried out in a conventional fixed-bed reactor. The sample (usually 100 mg), mixed with carborundum (SiC, 1.5 g, granulometry 210 µm) was *in situ* prereduced under 60 mL min^{-1} of H_2 at 650 °C for 1 h. After reduction, the reaction gas mixture was introduced at 575 °C at a flowrate of 100 mL min^{-1}. The gas mixture was composed of 50% C_3H_8, 45% N_2 and 5% H_2 corresponding to a molar ratio of 10:9:1. In these conditions, the maximum conversion calculated at the thermodynamic equilibrium is 46%. It was checked that experiments were performed in a kinetic regime. The weight hourly space velocity ($g_{propane}$ (g_{cat} h)$^{-1}$) was equal to 55 h^{-1}. These reaction conditions, especially the high C_3H_8/H_2 ratio, were chosen in order to favour the deactivation process and thus better see the effect of the addition of K. The flowrate at the outlet was measured on line using a Ritter Gas Meter. The outlet gas composition was analysed by an online Agilent 7820A gas chromatography equipped with an FID and HP-Al_2O_3/KCl capillary column. Propane conversion (X), activity (a), yield to each product C_xH_y (Y) and selectivity to propene (S) were calculated as follows:

$$X\,(\%) = \frac{F_{C_3H_8 in} - F_{C_3H_8 out}}{F_{C_3H_8 in}} \times 100 \qquad \text{(Eq. 2)}$$

$$a(\text{mol } h^{-1}\ g_{Pt}^{-1}) = \frac{X \times F_{C_3H_8 in}}{m \times \%_{Pt}} \qquad \text{(Eq. 3)}$$

$$Y_{CxHy}\,(\%) = \frac{x \times F_{C_xH_y}}{3 \times F_{C_3H_8}} \times 100 \qquad \text{(Eq. 4)}$$

$$S_{C3H6}\,(\%) = \frac{F_{C_3H_6 out}}{F_{C_3H_8 in} - F_{C_3H_8 out}} \times 100 \qquad \text{(Eq. 5)}$$

where $F_{C_3H_8}$ corresponds to the molar flowrate of propane (mol h^{-1}), and $F_{C_xH_y}$ refers to the molar flow rate of each product identified at the outlet (C_3H_6, C_2H_6, C_2H_4 and CH_4); *in* and *out* the molar flowrate at the inlet and at the outlet, respectively; *x* and *y* the number of carbon and hydrogen atoms in the molecule, respectively; *m* the mass of catalyst and $\%_{Pt}$ the percentage of platinum in wt.% in the catalyst. The yield in carbon Y_C was calculated by difference between propane conversion and the sum of the yields of the gaseous products. The percentage of propene in gas phase was calculated by dividing the yield in propene by the sum of the yields of all the products identified in gas phase.

The deactivation parameter ΔX was calculated by difference between the initial and final conversion as the following:

$$\Delta X\,(\%) = X_i - X_f \qquad \text{(Eq. 6)}$$

where i and f stand for initial and final.

3. Results

3.1. Physical and chemical properties of the supports and catalysts

The main characteristics of the supports are given in Table 1. While the actual K content is in agreement with the nominal one, the Pt content is inferior to the nominal value due to the deposition method. The BET surface area of all samples is of 200 ± 10 $m^2\ g^{-1}$ whatever the sample, showing that the deposition of K and Pt has no effect on the textural properties of the alumina support.

Table 1. Characteristics of the Al_2O_3, modified Al_2O_3 and supported Pt catalysts

Sample	K content[(a)] (wt.%)	K content[(a)] (mol.%)	BET Surface area (m^2 g^{-1})	Pt content (wt.%)[(a)]	$a_{rel.isom}$ (%)[(b)]	Concentration of LAS (µmol g^{-1})[(c)]	LAS distribution[(d)]		
							Weak sites (%)	Medium sites (%)	Strong sites (%)
Al_2O_3	-	-	206	-	100.0	333	50	27	23
Al_2O_3-0.5K	0.59	0.41	202	-	0.7	247	58	31	11
Al_2O_3-4K	3.17	2.21	192	-	0.2	n.d.[(e)]	n.d.	n.d.	n.d.
0.3Pt/Al_2O_3	-	-	191	0.22	69.0	275	59	19	22
0.3Pt/Al_2O_3-0.5K	0.39	0.27	199	0.22	2.3	221	62	27	11
0.2Pt/Al_2O_3-0.5K	0.39	0.27	195	0.15	1.8	n.d.	n.d.	n.d.	n.d.
0.1Pt/Al_2O_3-0.5K	0.44	0.30	187	0.10	1.2	n.d.	n.d.	n.d.	n.d.

[(a)] Standard deviation: ± 10%
[(b)] Characteristic of the Brønsted acidity and corresponding to the activity of the sample divided by the one of Al_2O_3 in 33DMB1 isomerization
[(c)] Calculated from the results of pyridine FTIR from the surface area of the peak at 1455 cm^{-1}
[(d)] Calculated from the results of pyridine FTIR by difference of the spectrum measured after thermodesorption at 150, 250 and 350 °C
[(e)] n.d.: not determined

The XRD patterns of the Al_2O_3 and Al_2O_3-K supports (Fig. 1) are typical of γ-Al_2O_3 with no diffraction line corresponding to potassium oxide demonstrating that, whatever the potassium loading, potassium does not modify the alumina structure and is probably well dispersed on the alumina support.

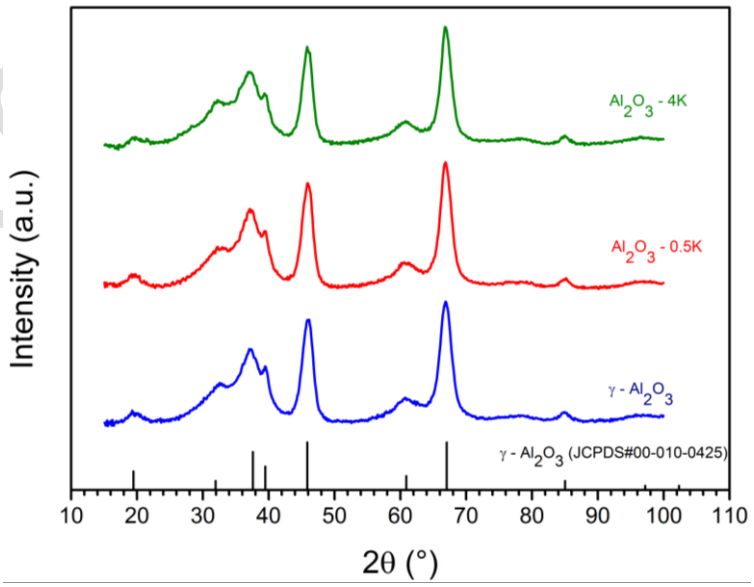

Fig. 1. XRD patterns of Al_2O_3, Al_2O_3-0.5K, Al_2O_3-4K, and γ-Al_2O_3 reference.

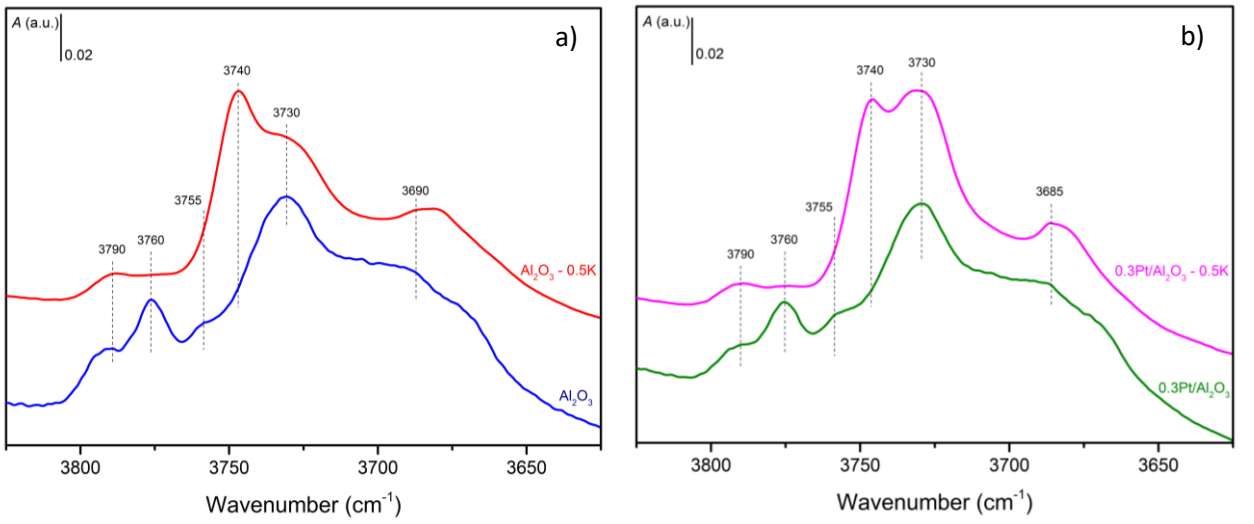

Fig. 2. FTIR spectra in the OH stretching region after pretreatment under vacuum at 500 °C of (a) Al_2O_3 and Al_2O_3-0.5K; (b) 0.3Pt/Al_2O_3 and 0.3Pt/Al_2O_3-0.5K.

The FTIR reference spectra of the supports in the ν(OH) region (3600-3800 cm^{-1} range), are displayed in Fig. 2a. The spectrum of Al_2O_3 is typical of transitional gamma alumina, with 5 bands at 3790, 3760, 3755, 3730 and 3690 cm^{-1} attributable to the stretching of OH groups coordinated to Al ions [48,49], either linearly or bridged to two or three Al ions. All bands, except the one at 3690 cm^{-1}, are attributable to OH terminal species with some acidic character [49]. The band generally identified in the 3760-3775 cm^{-1} range is ascribable to the most reactive and highly labile OH species at the alumina surface and is very sensitive to the doping by K [49-51]. When small amount of potassium is added to Al_2O_3, the spectrum is modified, with the appearance of a new band at 3740 cm^{-1} and the disappearance of the band at 3760 cm^{-1}. The same trend was obtained by Montanari *et al.* [52], but contrary to their results no band attributable to OH stretching of KOH species, which should appear in the 3720-3712 cm^{-1} range, is observed. This difference could be explained by the lower potassium loading, 5.4 wt.% in [52], and 0.59 wt.% in the present study. Consequently, a small amount of K is sufficient to suppress the band ascribed to the most reactive OH species without creating new bands due to the presence of KOH. When Pt is added on the supports (Fig. 2b), its effect depends on the presence or not of K. There

is only a minor modification of the spectrum of the bare Al_2O_3 support, with a slight decrease of the total surface area. On the Al_2O_3-0.5K support, the addition of Pt does not modify the surface area of the bands at 3790 cm^{-1} and 3740 cm^{-1}, while the surface area of the band at 3730 cm^{-1} is strongly enhanced and the one at 3690 cm^{-1} slightly decreases. The increase of the band at 3730 cm^{-1} could be explained by the loss of a part of K due to the deposition of Pt in solution in exchange conditions and then filtration. As a result, the initial K loading, 0.59 wt.% in Al_2O_3-0.5K, falls to 0.39 wt.% in Pt/Al_2O_3-0.5K, which represents a loss of more than 40% of K. As this band is attributable to acidic OH species, an increase of the Brønsted acidity is probable.

The surface acidity of the supports and catalysts was determined by FTIR of adsorbed pyridine. Spectra obtained after pyridine adsorption and thermodesorption at 150 °C and subtraction of the reference spectrum are presented in Fig. 3.

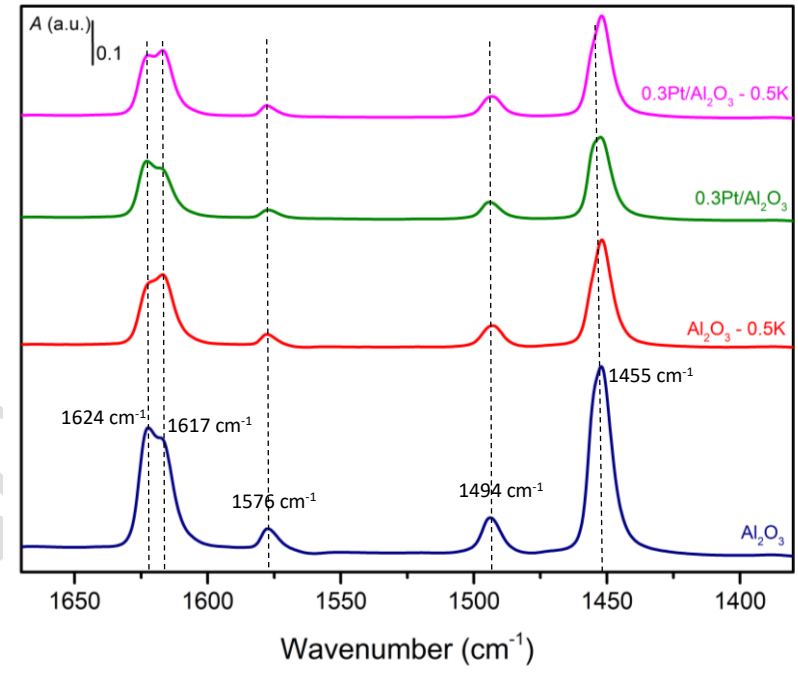

Fig. 3. FTIR spectra after pyridine desorption at 150 °C for Al_2O_3, Al_2O_3-0.5K, 0.3Pt/Al_2O_3 and 0.3Pt/Al_2O_3-0.5K.

Whatever the sample, two bands are visible in the ν8a region, at *ca.* 1624 and 1617 cm^{-1}, ascribed to strong tetrahedral coordinatively unsaturated (cus) Al^{3+} LAS and medium octahedral cus Al^{3+} LAS, respectively [53,54]. It is interesting to note that the band at 1624 cm^{-1} is predominant on the Al_2O_3 and 0.3Pt/Al_2O_3 samples, while on the two Al_2O_3-0.5K samples the contrary is observed, indicating that acid sites are stronger on Al_2O_3 and 0.3Pt/Al_2O_3 than on Al_2O_3-0.5K and 0.3Pt/Al_2O_3-0.5K. It is also important to note that, even if the band at 1617 cm^{-1} becomes more pronounced, both bands are decreased when K is added to Al_2O_3, indicating that K is deposited on both types of LAS sites but preferentially on the tetrahedral Al^{3+} ones in accordance with the results of de Miguel et al. [55]. The ν19b vibration band at *ca.* 1455 cm^{-1}, also attributable to LAS, allows their quantification. Results reported in Table 1 show the number of LAS decreases in the following order: Al_2O_3 > 0.3Pt/Al_2O_3 > Al_2O_3-0.5K > 0.3Pt/Al_2O_3-0.5K and their distribution confirms the trend observed from the ν8a band, with a higher proportion of strong LAS on the not modified Al_2O_3 samples than on the Al_2O_3-0.5K samples, which contain a higher proportion of weak and medium LAS. Another band at 1576 cm^{-1} is attributable to LAS, while no band at 1640 or 1545 cm^{-1} is visible, indicating that whatever the sample, there are no Brønsted acid sites (BAS) strong enough to protonate the adsorbed pyridine. Finally, the band at 1494 cm^{-1}, which is usually attributed to BAS and LAS, corresponds to LAS in the present case.

As the weak BAS cannot be characterized on the based-alumina samples by pyridine adsorption, 33DMB1 isomerization was used to qualitatively evaluate them. Results of Table 1 show that 0.59 wt.% of K (Al_2O_3-0.5K sample) are sufficient to virtually suppress the isomerization activity, which is less than 1% of the activity of the bare alumina support and not so different from the value determined for Al_2O_3-4K. This result is in accordance with the FTIR spectra relative to the OH range where it was shown that a low amount of K is sufficient to suppress the most active OH species. When Pt is added on bare alumina, a decrease of the isomerization activity is observed, from 100% to 69% while on the Al_2O_3-0.5K support, there is a slight increase, which could be due to a loss of potassium

and also to the deposition of platinum since this increase is all the more important as the Pt content increases. This result is in accordance with the evolution of the OH band at 3730 cm^{-1} observed between the FTIR spectra of the Pt/Al_2O_3-0.5K and Al_2O_3-0.5K samples. The $a_{rel.isom}$ value increases linearly from 1.2 to 2.3% when the Pt content varies from 0.1 to 0.3 wt.%, and an extrapolation to 0 wt.% of Pt gives a virtual $a_{rel.isom}$ value of 0.66%, similar to the measured value of 0.7% for Al_2O_3-0.5K. Consequently, the increase in the Brønsted acidity is due to the presence of Pt and not to the loss of K. An increase in 33DMB1 isomerization activity, due to the presence of oxidized Pt species at the metal-support interface, was observed by Martin and Duprez [47] but after a calcination and not after a reductive pretreatment as in the present case. Consequently, it can be inferred that, in the present study, a part of Pt is only partially reduced during the pretreatment, indicating a strong metal-support interaction with electron deficient species at the metal support interface and probably a high dispersion of Pt species.

In order to characterize platinum dispersion, H_2 chemisorption was performed and very high values (H/Pt>1.5) were obtained. As similar results were obtained by performing H_2 chemisorption at low temperature (- 77 °C) and CO chemisorption, hydrogen spillover phenomenon from Pt towards the alumina support cannot explain these high H/Pt values. Freel [56] obtained a value of H/Pt = 1.35 for 2 wt.%Pt/SiO_2, and more recently we reported a value of H/Pt = 1.49 for 1 wt.%Pt/Al_2O_3 [52]. A H/Pt value of 1.85 was obtained by calculation based on a geometrical approach considering perfect cuboctahedron Pt clusters. This high value corresponded to the smallest crystallite of 13 atoms, with a dispersion value of 0.92 since only 12 atoms are accessible [58]. It was demonstrated by *in situ* X-ray absorption spectroscopy, STEM analyses and DFT calculation [59] that Pt single atoms observed after oxidation of just impregnated 0.3 wt.%Pt/Al_2O_3 sample are very mobile when heated under H_2 atmosphere and aggregate to form subnanometric clusters. This mobility is explained by the disconnection of Pt atoms from the support due to the presence of interfacial hydrogen between the metal cluster and the support when a dimer of Pt is formed, leading to a Pt_2H_6 species with H/Pt = 3.

Except this maximum value, the H/Pt ratio increases from 2 for Pt_1 to 2.5 for Pt_{13} cluster. Thus, the very high H/Pt values obtained in the present study could be attributed to highly dispersed Pt atoms. To check this point, TEM images of $0.3Pt/Al_2O_3$ are presented in Fig. 4. It is important to specify that only few particles were visible and their diameter was in the 0.4-1.6 nm range, with a maximum of particles with a diameter of 0.8 nm, confirming the high dispersion of Pt, while the non-visible Pt species are highly dispersed. Similar results were obtained by Zhang *et al.* [42] for 0.1 and 0.3 wt.%Pt supported on hierarchically structured nanoalumina, while only 16% of Pt dispersion was observed on 0.3 wt.%Pt/Al_2O_3 by Yu et al. [21]. On the other samples, no Pt particles were seen on the alumina support confirming the very high dispersion of Pt on Al_2O_3-K samples.

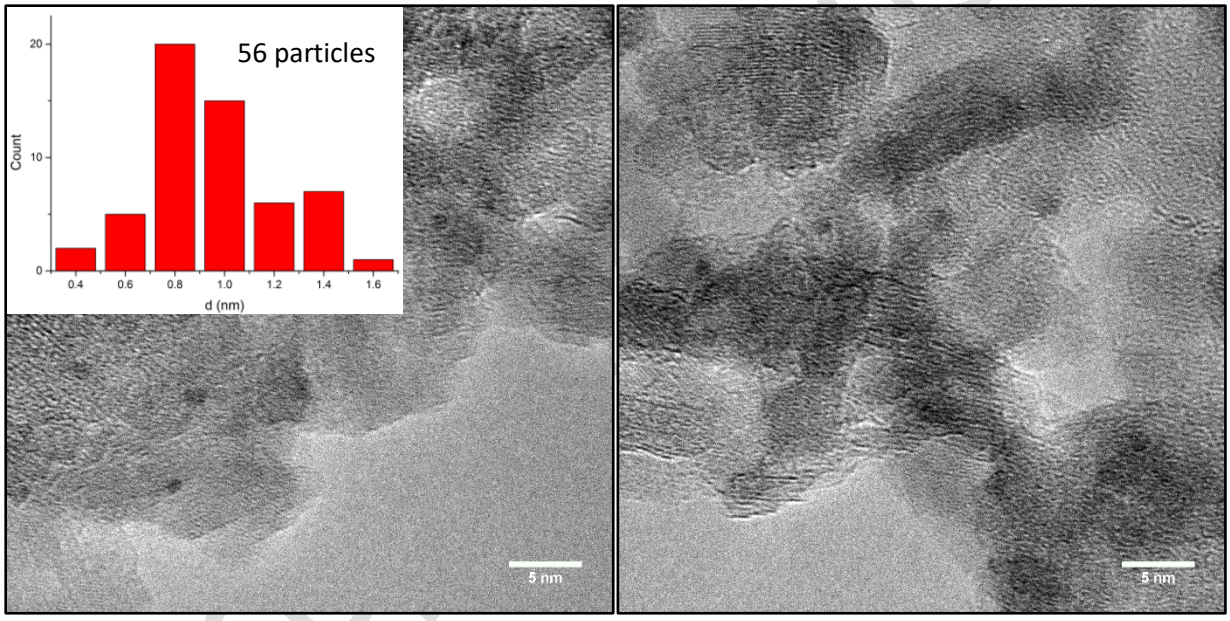

Fig. 4. TEM image of $0.3Pt/Al_2O_3$ and distribution of particle size (inserted figure) for visible particles.

3.2. Propane dehydrogenation

Results obtained in propane dehydrogenation in the presence of the various catalysts are reported in Table 2. It should be noted that the supports alone, Al_2O_3 and Al_2O_3-0.5K, are not able to convert propane. In addition, the calculation at the thermodynamic equilibrium allows determining that the maximum propane conversion in the experimental conditions is 46% when considering that propane

is only converted into propene and dihydrogen. The evolution of the conversion and the percentage of propene in gas phase as a function of time are displayed in Fig. 5.

Table 2. Performance of the catalysts for propane dehydrogenation (T = 575 °C, 50% C_3H_8, 5% H_2, 45% N_2)

Catalyst	X_i [(a)] (%)	X_f [(a)] (%)	ΔX (%)	Coke content (wt.%)	a_i (mol h^{-1} g_{Pt}^{-1})	TOF_i [(b)] (s^{-1})	Y_i [(c)] (%)					C_3H_{6i} in gas phase [(c)] (%)	S_i C_3H_6 [(c)] (%)
							CH_4	C_2H_6	C_2H_4	C_3H_6	C		
0.3Pt/Al_2O_3	27	9	18	1.01	129 ± 14	7.0 ± 0.8	0.64	0.45	0.51	14.27	11.20	90	53
0.3Pt/Al_2O_3-0.5K	20	14	6	0.63	99 ± 15	5.4 ± 0.8	0.32	0.21	0.42	12.21	6.98	93	61
0.2Pt/Al_2O_3-0.5K	17	8	9	0.59	130 ± 23	7.0 ± 1.3	0.22	0.12	0.32	10.82	5.14	94	65
0.1Pt/Al_2O_3-0.5K	13	4	7	0.43	147 ± 33	7.9 ± 1.8	0.14	0.06	0.23	9.10	1.42	95	83

[(a)] Standard deviation: ± 3
[(b)] TOF: Turnover frequency value calculated from the initial activity a_i considering 100% of Pt sites accessible.
[(c)] Values of initial yields, initial percentage in propene in gas phase and initial selectivity, obtained at the beginning of the reaction.

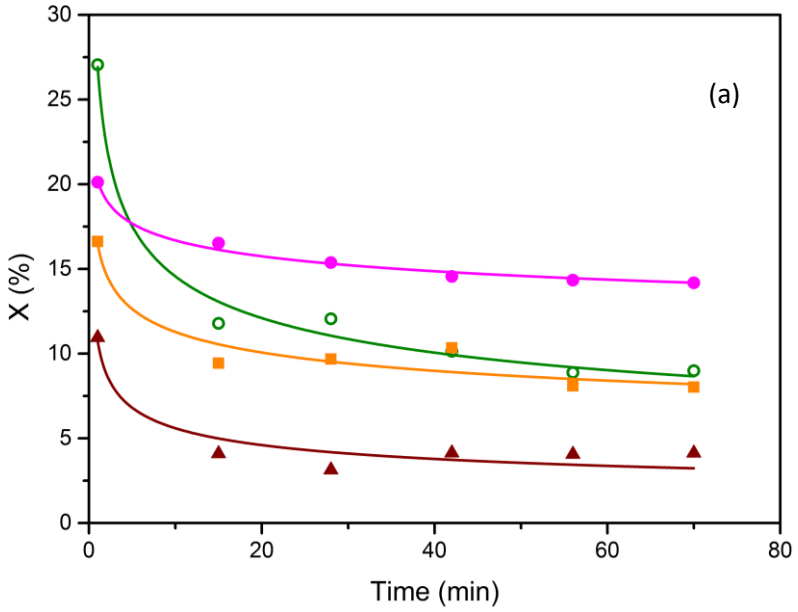

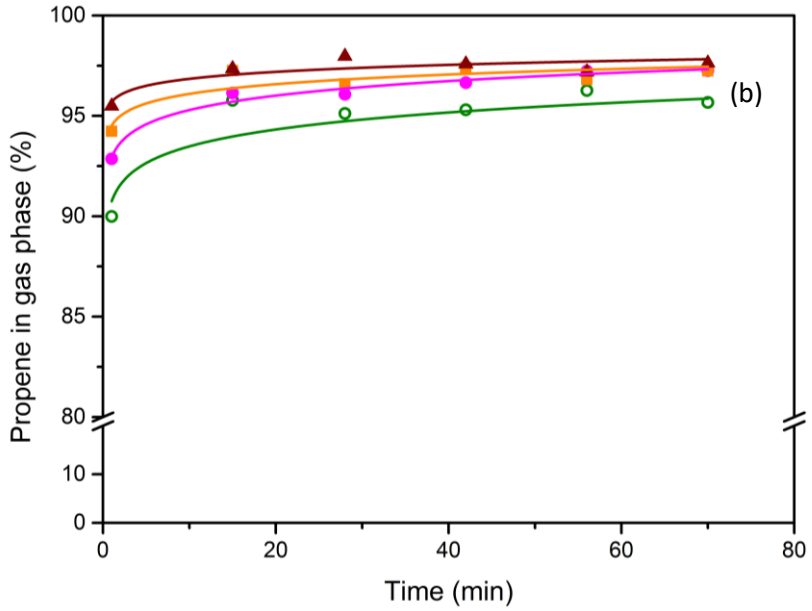

Fig. 5. (a) Evolution of propane conversion and (b) percentage of propene in gas phase as a function of time-on-stream during propane dehydrogenation in the presence of 100 mg of 0.3Pt/Al_2O_3 (○), 0.3Pt/Al_2O_3-0.5K (●), 0.2Pt/Al_2O_3-0.5K (■), 0.1Pt/Al_2O_3-0.5K (▲) (T = 575 °C, 50% C_3H_8, 5% H_2, 45% N_2).

For the same metal loading, 0.3 wt.%, Pt/Al_2O_3 catalyst exhibits an initial activity in propane conversion slightly higher to that of Pt/Al_2O_3-0.5K, and in line with that of 1 wt.%Pt/Al_2O_3 with also a very high dispersion (H/Pt = 1.44) [40]. As the value of H/Pt, reflecting metal accessibility, is very high, an apparent TOF value was calculated considering that all the Pt atoms are accessible to the reactants (100% dispersion). It appears that the TOF values can be considered similar for both 0.3wt.%Pt samples given the standard deviation. Since the presence of K does not modify the activity of Pt sites for propane conversion, it can be inferred that there is no interaction between Pt and K. This result is different from that obtained by Cortright and Dumesic [60] comparing Pt/SiO_2 and Pt/K/SiO_2 for isobutane dehydrogenation, but in their case K was impregnated onto the Pt/SiO_2 sample. The same trend was observed with boron or sodium as promoters for Pt/Al_2O_3 [23,61]. A decrease in activity for propane dehydrogenation was observed when boron was introduced after Pt while there is no change

in TOF value when boron is deposited on alumina before Pt [61], which can be explained by a geometric effect of B deposited onto Pt nanoparticles. It can be concluded that the order of introduction of K on the catalyst before or after Pt deposition plays an important role on the activity for propane dehydrogenation. Furthermore, the K-modified sample displays a higher selectivity to propene, which is due not only to the decrease of the yields in methane, ethane and ethylene, but more importantly to the decrease of the yield in carbon and percentage of coke deposited (Table 2). As a consequence, the deactivation is by far less important for 0.3Pt/Al_2O_3-0.5K than for 0.3 Pt/Al_2O_3 as illustrated by the decrease of the deactivation parameter ΔX (Table 2). The deactivation phenomenon occurs mainly at the beginning of the catalytic test for both 0.3Pt catalysts (Fig. 5a). It is accompanied by an increase in the amount of propene in gas phase as the conversion decreases (Fig. 5b). Consequently, the change in propene selectivity between 0.3Pt/Al_2O_3-0.5K and 0.3 Pt/Al_2O_3 could be due to the change in conversion, and it is not possible to conclude at this stage on a beneficial effect or not on the selectivity of carbon deposition and of the presence or not of K on the support.

On the Al_2O_3-0.5K support, when the actual Pt content decreases from 0.22 to 0.1 wt.%, the conversion and the yield in the various products obviously decrease in the same way. Taking into account the Pt loading, the apparent TOF values reported in Table 2 would seem to indicate that the activity of Pt sites slightly increases when the Pt content decreases. As this result could be due to the increase in the standard deviation as the Pt content decreases, catalytic tests were performed with the 0.1Pt/Al_2O_3-0.5K and 0.2Pt/Al_2O_3-0.5K samples by increasing the catalyst loading in order to have the same amount of active phase in the reactor as for the 0.3Pt/Al_2O_3-0.5K sample, while adjusting the amount of carborundum to maintain constant the height of the catalytic bed. In this case, the TOF values are equal to 4.0 ± 0.7 s^{-1} for 0.1Pt/Al_2O_3-0.5K and 4.3 ± 0.7 s^{-1} for 0.2Pt/Al_2O_3-0.5K, similar to that of 0.3Pt/Al_2O_3-0.5K, showing no effect of the metal content, which is an expected result since all the catalysts are composed of ultradispersed Pt species. Thus, for highly dispersed diluted Pt atoms, it can be supposed that all the exposed Pt sites present similar activities, in accordance with the results of

Biloen *et al*. obtained by diluting 0.5 to 14% of Pt atoms in gold [62]. As far as propene formation is concerned, the increase of the percentage of propene in gas phase is once again linked to the fall of the conversion whatever the Pt content (Fig. 5b). Thus it is not possible to conclude on a beneficial effect on the selectivity of the addition of K and decrease in Pt content from the results presented in Table 2. To clarify this point, the evolution of the percentage of propene in gas phase during time-on-stream is reported as a function of the conversion for all the catalysts in Fig. 6.

Fig. 6 clearly highlights that the percentage of propene in gas phase is linked to the value of the conversion and not to the catalyst composition, since it decreases when the conversion increases in the same manner whatever the nature of the catalyst.

Regarding the effect of the Pt content on the stability of the catalysts supported on Al_2O_3-0.5K, it can be seen that the drop in conversion is similar whatever the Pt content (Fig. 5), which is confirmed by the similar deactivation parameter and amount of carbon deposited (Table 2). Thus, it can be concluded that there is no apparent link between conversion and deactivation, contrary to what was observed for propene production.

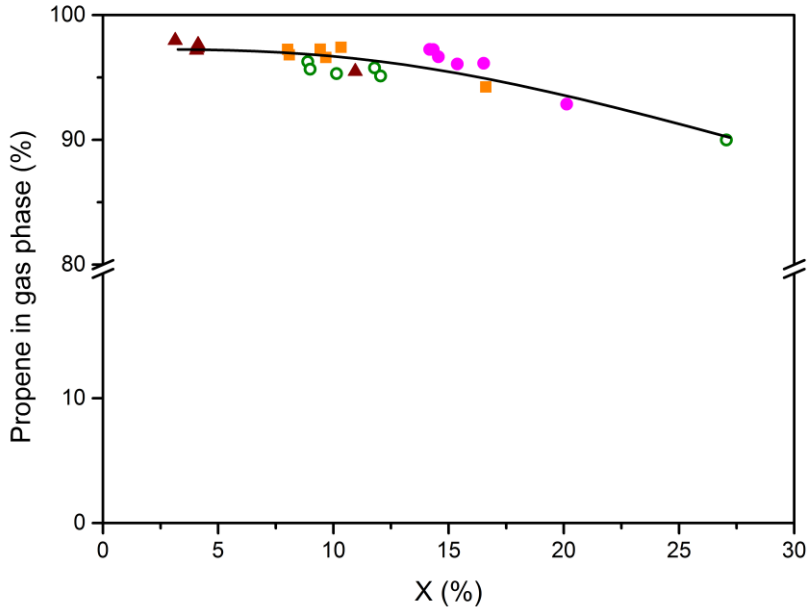

Fig. 6. Evolution of the percentage of propene in gas phase as a function of the propane conversion during time-on-stream over 0.3Pt/Al_2O_3 (○), 0.3Pt/Al_2O_3-0.5K (●), 0.2Pt/Al_2O_3-0.5K (■), 0.1Pt/Al_2O_3-0.5K (▲) (T = 575 °C, 50% C_3H_8, 5% H_2, 45% N_2, time-on-stream = 70 min).

Coke deposition occurs whatever the catalyst, with more carbon on 0.3Pt/Al_2O_3 (1.01 wt.%) than on the 0.1-0.3Pt series supported on modified alumina (0.4-0.65 wt.%), and is probably responsible in part for the deactivation. In order to determine the temperature of coke combustion, indicative of the kind of carbon species deposited on the catalysts, the samples were also analyzed by TG/DTG after reaction. An example of a TG/DTG analysis profile, corresponding to 0.3Pt/Al_2O_3 after catalytic test, is presented in Fig. 7a. It can be seen from the TG curve that there is a continuous decrease of weight from RT up to 900 °C, with major weight losses, identified from DTG curve, at *ca.* 100 °C, corresponding probably to the removal of water and at *ca.* 400 °C, which could be ascribed to carbon species, as confirmed by the formation of CO_2 identified by mass spectrometry (results not shown). Given the temperature of oxidation, these coke species are probably at the Pt-Al_2O_3 boundary [61,63]. It is also important to outline that a continuous formation of CO_2 is observed from RT to ca. 550 °C. The analysis by mass spectrometry also confirmed that water is mostly formed around 100 °C but also continuously at higher temperature with another important formation around 400 °C when CO_2 is formed. Thus, the continuous loss of weight observed on the TG profile is in part due to the dehydroxylation of alumina which occurs in parallel to carbon oxidation, which is confirmed by the TG/DTG profile of the bare Al_2O_3 support (Fig. 7b) and in accordance with [64].

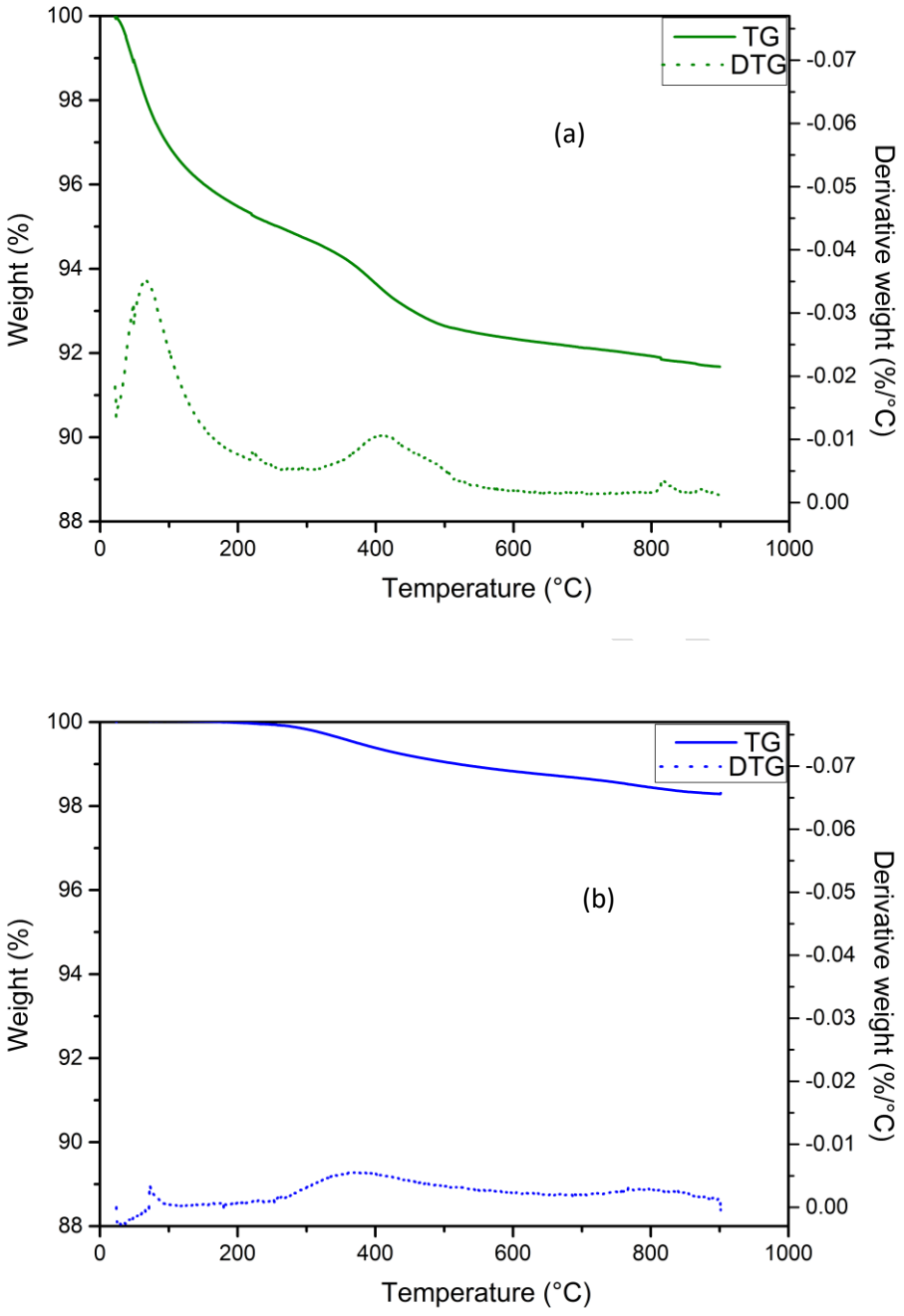

Fig. 7. TG/DTG profiles after propane dehydrogenation reaction of 0.3Pt/Al_2O_3 (a) and bare Al_2O_3 (b).

This important dehydroxylation is due to the high surface area of the Al_2O_3 chosen for this study. As the amount of hydroxyl groups is in the range 12-16 OH per nm^2 on γ-Al_2O_3 after outgassing at 100 C and is inferior to 3 OH per nm^2 after outgassing at 700 C [65], *ca.* 9 OH per nm^2 should be lost between 100 and 700 °C, which corresponds to a loss of weight of roughly 5 wt.%, i.e. 0.3 mol.% for an Al_2O_3

of 200 m^2 g^{-1} as the one chosen for the present study. Consequently, on bare alumina the major losses are observed at roughly the same temperatures as those for the used Pt/Al_2O_3 sample, making it impossible to discriminate coke combustion from dehydroxylation phenomenon from the TG/DTG profiles.

Finally, during the catalytic test, a sintering of metal particles also occurs, as illustrated by TEM image in Fig. 8, a majority of particles being of 1.0 nm instead of 0.8 nm for the fresh $0.3Pt/Al_2O_3$ catalyst (Fig.8a) and some particles with diameters between 0.8 and 1.2 nm for $0.3Pt/Al_2O_3$-0.5K while they were not visible on the fresh $0.3Pt/Al_2O_3$-0.5K sample. Coke is also clearly seen in the images, on the support or in the vicinity of a metal nanoparticle. The sintering is also responsible, as carbon deposit, of the deactivation phenomenon whatever the catalyst.

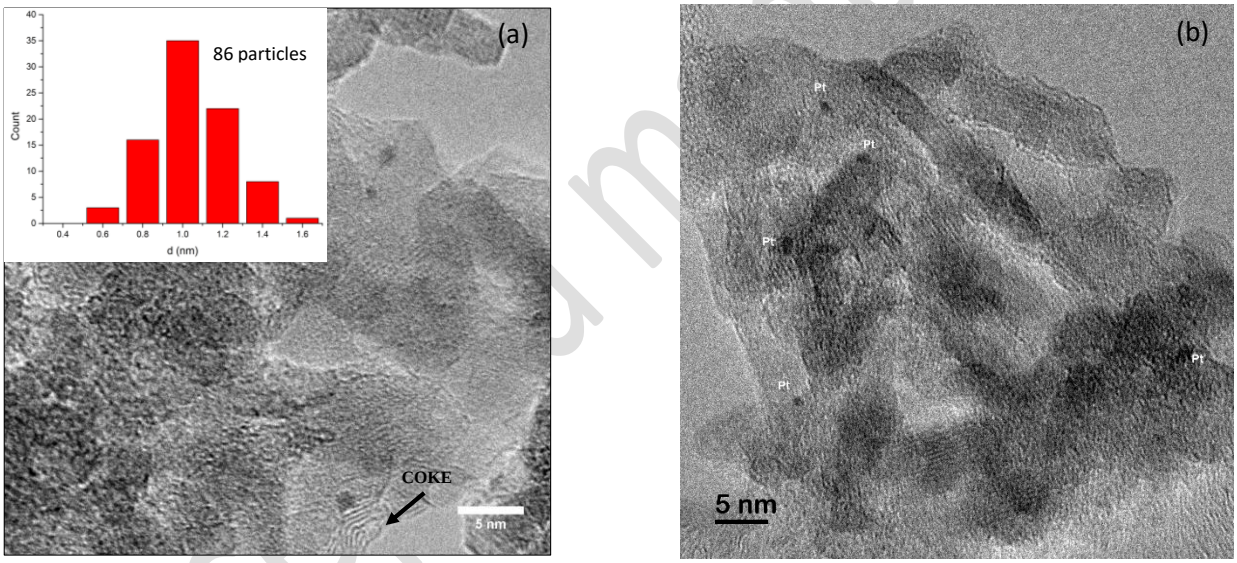

Fig. 8: TEM image and distribution of particle size (inserted figure) for $0.3Pt/Al_2O_3$ (a) and $0.3Pt/Al_2O_3$-0.5K (b) after catalytic test.

4. Conclusion

γ-Al_2O_3 modified by various K contents (0.5K and 4K in wt.%) were studied. Pt catalysts with various platinum contents (0.1, 0.2 and 0.3 wt.%) were then prepared on Al_2O_3 or Al_2O_3-0.5K and

characterized with the aim of better understanding the effect of platinum and potassium on the catalytic performances in propane dehydrogenation. It was shown that, whatever the K content, K deposition has no effect on the textural properties of the alumina support at the surface of which it is well dispersed modifying the nature of its hydroxyl groups and consequently decreasing its Brønsted acidity. The presence of K also decreases the Lewis acid sites number as well as their distribution due to the loss of strong Lewis acid sites. Thus, in accordance with the literature, it was confirmed that the addition of K decreases the acidity of the alumina support. As a consequence, 0.3Pt/Al_2O_3-0.5K is more stable during propane dehydrogenation than its not modified counterpart, 0.3Pt/Al_2O_3. On the Al_2O_3-0.5K support, the decrease in Pt content does not modify the activity nor the deactivation process. This study also allows us to conclude that low amounts of K are sufficient to suppress the acidity of the alumina detrimental to the stability. For Pt monometallic catalysts, the presence of K and the Pt content have no apparent effect on the selectivity to propene, which depends strongly on the conversion. Then, the challenge consists in increasing propane conversion while maintaining high propene selectivity. The improvements of the catalytic formulations by addition of promoters to limit deactivation and increase propene selectivity should start from Pt/Al_2O_3-0.5K with low Pt contents while high Pt and K contents are the most usually described in the literature.

Acknowledgment:

The authors acknowledge financial support from the European Regional Development Fund (ERDF) and Région Nouvelle Aquitaine. This work pertains to the French Government program «Investissements d'Avenir» (EUR INTREE, reference ANR-18-EURE-0010). The authors thank Stéphane Pronier for the acquisition of TEM images.

References

1. J.J.H.B. Sattler, J. Ruiz-Martinez, E. Santillan-Jimenez, B.M. Weckhuysen, Chem. Rev. 114 (2014) 10613–10653.

2. L. Deng, T. Shishido, K. Teramura, T. Tanaka, Catal. Today 232 (2014) 33-39.

3. H. Xiong, S. Lin, J. Goetze, P. Pletcher, H. Guo, L. Kovarik, K. Artyushkova, B.M. Weckhuysen, A.K. Datye, Angew. Chem. Int. Ed, 56 (2017) 8986-8991.

4. N. Prakash, M-H. Lee, S. Yoon, K-D. Jung, Catal. Today 293-294 (2017) 33-41.

5. E.J. Jang, J. Lee, H.Y. Jeong, J.H. Kwak, Appl. Catal. A 572 (2019) 1-8.

6. Z-P. Hu, D. Yang, Z. Wang, Z-Y. Yuan, Chin. J. Catal. 40 (2019) 1233-1254.

7. J-W. Jung, W-I. Kim, J-R. Kim, K. Oh, H.L. Koh, Catalysts 9 (2019) 446-458.

8. Y. Nakaya, J. Hirayama, S. Yamazoe, K. Shimizu, S. Furukawa, Nature Com. 11 (2020) 2838-2844.

9. K. Searles, K.W. Chan, J.A. Mendes Burak, D. Zemlyanov, O. Safonova, C. Copéret, J. Am. Chem. Soc. 140 (2018) 11674-11679.

10. X. Chen, M. Ge, Y. Li, Y. Liu, J. Wang, L. Zhang, Appl. Surf. Sc. 490 (2019) 611-621.

11. M.D. Marcinkowski, M.T. Darby, J. Liu, J.M. Wimble, F.R. Lucci, S. Lee, A. Michaelides, M. Flytzani-Stephanopoulos, M. Stamatakis, E.C.H. Sykes, Nature Chem. 10 (2018) 325-332.

12. Y. Zhang, Y. Zhou, J. Shi, S. Zhou, X. Sheng, Z. Zhang, S. Xiang, J. Mol. Catal. A 381(2014) 138-147.

13. C. Sun, J. Luo, M. Cao, P. Zheng, G. Li, J. Bu, Z. Gao, S. Chen, X. Xie, J. Energy Chem. 27(2018) 311-318.

14. F.T. Zangeneh, S. Mehrazma, S. Sahebdelfar, Fuel Process. Technol. 109 (2013) 118-123.

15. L. Shi, G.M. Deng, W.C. Li, S. Miao, Q.N. Wang, W.P. Zhang, A.H. Lu, Angew. Chem. Int. Ed. 54 (2015) 13994-13998.

16. Y.L. Shan, T. Wang, Z.J. Sui, Y.A. Zhu, X.G. Zhou, Catal. Commun. 84 (2016) 85-88.

17. H. Zhu, D.H. Anjum, Q. Wang, E. Abou-Hamad, L. Emsley, H. Dong, P. Laveille, L. Li, A.K. Samal, J.M. Basset, J. Catal. 320 (2014) 52-62.

18. G.Q. Ren, G.X. Pei, Y.J. Ren, K.P. Liu, Z.Q. Chen, J.Y. Yang, Y. Su, X.Y. Liu, W.Z. Li, T. Zhang, J. Catal. 366 (2018) 115-126.

19. X. Fan, J. Li, Z. Zhao, Y. Wei, J. Liu, A. Duan, G. Jiang, Catal. Sci. Technol. 5 (2015) 339-350.

20. B. Li, Z. Xu, W. Chu, S. Luo, F. Jing, Chin. J. Catal. 38 (2017) 726-735.

21. C. Yu, Q. Ge, H. Xu, W. Li, Catal. Lett. 112 (2006) 197-201.

22. C. Byron, S. Bai, G. Celik, M.S. Ferrandon, C. Liu, C. Ni, A. Mehdad, M. Delferro, R.F. Lobo, A.V. Teplyakov, ACS Catal., 10 ((2020) 1500-1510.

23. S.A. Bocanegra, A.A. Castro, A. Guerrero-Ruíz, O.A. Scelza, S.R. de Miguel, Chem. Eng. J. 118 (2006) 161-166.

24. G.J. Siri, G.R. Bertolini, M.L. Casella, O.A. Ferretti, Mater. Lett. 59 (2005) 2319-2324.

25. Y. Minemura, M. Kuriyama, S.-I. Ito, K. Tomishige, K. Kunimori, Catal. Comm. 7 (2006) 623.

26. H. Liu, A. Jia, Yuwang, M. Luo, J. Lu, Chinese J Catal 36 (2015) 1976-1986.

27. Y. Wang, H.-H. Liu, S.-Y. Wang, M.-F. Luo, J.-Q. Lu, J. Catal. 311 (2014) 314-324.

28. J. Luo, F. Gao, D. H. Kim, C.H.F. Peden, Catal. Today 231 (2014) 164-172.

29. G. Avgouropoulos, E. Oikonomopoulos, D. Kanistras, T. Ioannides, Appl. Catal. B, 65 (2006) 62-69.

30. M-H. Lee, B.M. Nagaraja, P. Natarajan, N.T. Truong, K.Y. Lee, S. Yoon, K-D. Jung, Res. Chem. Intermed. 42 (2016) 123-140.

31. S. Zhao, B. Xu, L. Yu, Y. Fan, Chin. Chem. Lett. 29 (2018) 475-478.

32. J. Salmones, J-A. Wang, J.A. Galicia, G. Aguilar-Rios, J. Mol. Catal. A 184 (2002) 203-213.

33. H.N. Pham, J.J.H.B. Sattler, B.M. Weckhuysen, A.K. Datye, ACS Catal. 6 (2016) 2257-2264.

34. B.K. Vu, M.B. Song, I.Y. Ahn, Y-W. Suh, D.J. Suh, W-I. Kim, H-L. Koh, Y.G. Choi, E.W. Shin, Appl. Catal. A 400 (2011) 25-33.

35. L. Deng, H. Miura, T. Ohkubo, T. Shishido, Z. Wang, S. Hosokawa, K. Teramura, T. Tanaka, Catal. Sci. Technol. 9 (2019) 947-956.

36. G. Aguilar-Rios, P. Salas, M.A. Valenzuela, H. Armendariz, J.A. Wang, J. Salmones, Catal. Lett. 60 (1999) 21-25.

37. M. Aly, E.L. Fornero, A.R. Leon-Garzon, V.V. Galvita, M. Saeys, ACS Catal. 10 (2020) 5208-5216.

38. M. Santhosh Kumar, D. Chen, J.C. Walmsley, A. Holmen, Catal. Commun. 9 (2008) 747-750.

39. J. Zhu, M-L. Yang, Y. Yu, Y-A. Zhu, Z-J. Sui, X-G. Zhou, A. Holmen, D. Chen, ACS Catal. 5 (2015) 6310-6319.

40. A. Le Valant, S. Bouchet, A. Van Assche, C. Especel, F. Epron, J. Catal. 397 (2021) 64-74.

41. Z. Lu, R.W. Tracy, M.L. Abrams, N.L. Nicholls, P.T. Barger, T.Li, P.C. Stair, A.A. Dameron, C.P. Nicholas, C.L. Marshall. ACS Catal. 10 (2020) 13957-13967.

42. W. Zhang, H. Wang, J. Jiang, Z. Sui, Y. Zhu, D. Chen, X. Zhou, ACS Catal. 10 (2020) 12932-12942.

43. X. Li, Y. Zhou, B. Qiao, C. Wang, L. Cao, L. Li, J. Lin, X. Wang, J. Energ. Chem. 51 (2020) 14-20.

44. J.E. Samad, S. Hoenig, J.R. Regalbuto, ChemCatChem, 7 (2015) 3460-3463.

45. M. Guisnet, P. Ayrault, C. Coutanceau, M.F. Alvarez, J. Datka, J. Chem. Soc., Faraday Trans., 93 (1997) 1661-1665.

46. C. Kemball, H.F. Leach, B. Skundric, K.C. Taylor, J. Catal., 27 (1972) 416-423.

47. D. Martin, D. Duprez, J. Mol. Catal. A, 118 (1997) 113-128.

48. T.K. Phung, A. Lagazzo, M.A. Rivero Crespo, V. Sanchez Escribano, G. Busca, J. Catal. 311 (2014) 102-113.

49. G. Busca, Catal. Today 226 (2014) 2-13.

50. C. Morterra, G. Magnacca, Catal. Today 27 (1996) 497-532.

51. S. Srinivasan, C.R. Narayanan, A.K. Datye, Appl. Catal. A., 193 (1995) 289-308.

52. T. Montanari, L. Castoldi, L. Lietti, G. Busca, Appl. Catal. A 400 (2011) 61-69.

53. F. Can, A. Le Valant, N. Bion, F. Epron, D. Duprez, J. Phys. Chem. C, 112 (2008) 14145-14153.

54. A. Jordan, M.I. Zaki, C. Kappenstein, PCCP, 6 (2004) 2502-2512.

55. S.R. de Miguel, O.A. Scelza, A.A. Castro, J. Soria, Top. Catal. 1 (1994) 87-64.

56. J. Freel, J. Catal. 25 (1972) 149-160.

57. A. Le Valant, F. Drault, C. Maleix, C. Comminges, R. Beauchet, Y. Batonneau, L. Pirault-Roy, C. Especel, F. Epron, J. Catal. 367 (2018) 234-243.

58. A. Le Valant, C. Comminges, F. Can, K. Thomas, M. Houalla, F. Epron, J. Phys. Chem. C, 120 (2016) 26374-26385.

59. C. Dessal, A. Sangnier, C. Chizallet, C. Dujardin, F. Morfin, J.L. Rousset, M. Aouine, M. Bugnet, P. Afanasiev, L. Piccolo, Nanoscale, 11 (2019) 6897-6904.

60. R.D. Cortright, J.A. Dumesic, J. Catal. 157 (1995) 576-583.

61. M. Aly, E.L. Fornero, A.R. Leon-Garzon, V.V. Galvita, M. Saeys, ACS Catal. 10 (2020) 5208-5216.

62. P. Biloen, F.M. Dautzenberg, W.M.H. Sachtler, J. Catal. 50 (1977) 77-86

63. B.K. Yu, S.M. Bok, I.Y. Ahn, E.W. Shin, Catal. Lett. 133 (2009) 376-381.

64. R. Wischert, C. Copéret, F. Delbecq, P. Sautet, Angew. Chem. Int. Ed. 50 (2011) 3202-3205.

65. R. Wischert, P. Laurent, C. Copéret, F. Delbecq, P. Sautet, J. Am. Chem. Soc.134 (2012) 14430-14449.